Hindawi
Mathematical Problems in Engineering
Volume 2019, Article ID 6410704, 15 pages
https://doi.org/10.1155/2019/6410704

Research Article

Effect of Thermal Cycling on Operational Characteristics and Lifetime Prediction of Space Pulse Tube Refrigerator

Fubin Wan,[1] **Xun Chen**,[1] **Zhenhua Jiang**,[2] **and Yinong Wu**[2]

[1]*Laboratory of Science and Technology on Integrated Logistics Support, National University of Defense Technology, Changsha, Hunan 410073, China*
[2]*Shanghai Institute of Technical Physics, China Academy of Science, Shanghai 200084, China*

Correspondence should be addressed to Fubin Wan; wanfubin12@nudt.edu.cn

Received 23 July 2019; Accepted 4 September 2019; Published 29 September 2019

Academic Editor: Peter Dabnichki

This paper presents the operation status and results of ground thermal cycling test of pulse tube refrigerators (PTRs) for space application. Firstly, a thermal cycling degradation model was proposed by considering two physical mechanisms: contamination and fatigue damage. Then, a thermal cycling test scheme of two types of PTRs was designed and performed to demonstrate their long lifetime and high thermal stability. Two type A PTRs with cooling capacity of 1W@60 K and two type B PTRs with cooling capacity of 5W@80 K were continuously operated for about two years in a simulated vacuum thermal cycling environment. Effects of heat rejection temperature variation on thermal stability and dynamic performance of the PTRs were investigated. Furthermore, the thermal cycling degradation model was validated with the actual thermal cycling test data. Finally, the predicted pseudo-failure lifetime was acquired via experimental data and degradation model. Moreover, the estimated reliability of PTRs was obtained through using the Weibull distribution. The proposed thermal cycling test scheme and innovative lifetime prediction and reliability estimation method provide a quick and accurate approach for the cooler manufacturer to assess the lifetime and reliability of the space PTRs.

1. Introduction

Cryogenic technology has become more and more important as cryogenic detectors play a critical role in the fields of meteorological forecast, earth observation, and astronomical research. The long-life infrared detectors are required to operate at a cryogenic temperature in order to decrease background noise and provide high sensitivity and resolution [1–3]. Miniature mechanical cryocoolers have been greatly developed for cooling the detectors [4–6]. Among mechanical cryocoolers, the pulse tube refrigerators (PTRs) have been widely acknowledged as a new-generation space cryocooler for their advantages of long lifetime, low vibration, and compact structure for long-life space missions [7–10]. To satisfy the growing demand, PTRs not only should address the technical parameters but also must reach the requirements in term of temperature stability, operating reliability, and lifetime that critically affect the sensitive detectors. It is a great challenge for the PTRs which must maintain long-term stable operation with predictable performance despite a rigorous operating environment. The mission requirement of the cooling system is to keep the detectors at certain cryogenic temperatures with instability of less than 3 K for 8 years.

The PTRs installed on high orbit satellites are commonly subjected to a long-term repeated thermal cycling environment due to passing of the illuminated and shaded areas induced by solar eclipse and sun illumination in space. Previous studies [11–13] have shown that the heat reject temperature has a significant impact on the cooling performance and stability of the cryocoolers. For example, gaseous contamination, one of the major failure mechanisms of the cryocoolers, is strongly dependent on temperature changes [13]. Long-term periodic temperature change will ultimately produce a problem of instability and unreliable operation of the detectors. Unfortunately, only a sparse

number of papers [12, 14–16] reported the experimental and theoretical results about the performance of cryocoolers under thermal cycling environment. Nguyen et al. [12] presented the thermal cycling test data of a single-stage coaxial pulse tube cryocooler to demonstrate the long lifetime and high reliability of the cooler system. The cryocooler also showed excellent temperature stability when the reject temperature varied from 293 K to 300 K. Nast et al. [14] conducted a thermal vacuum cycle test to demonstrate the qualification of the pulse tube cryocooler to a technology readiness level of six. Cauquil et al. [15] performed a life test in thermal cycles between 293 K and 328 K on a serial production of Thales cryogenics RM2 coolers, and the mean time to failure of the coolers was 4900 hours. To demonstrate the 40000 hours designed lifetime of Sunpower M87 N cryocoolers, Shirey [16] et al performed thermal cycling tests on the cryocoolers with a temperature range of −20°C to 40°C that could be experienced on orbit. The space cryocoolers in the laboratory can achieve the required technical parameters such as cooling temperature and cooling power. But whether they can operate stably for more than 8 years in a dynamic space environment needs to be systematically investigated and demonstrated. To research the effect of a thermal cycling environment on the performance of the space PTRs, a set of experiments are performed and their thermal performance will be quantitatively presented in continuous operation conditions.

In this study, theoretical and experimental research on the thermal stability and lifetime of pulse tube refrigerators in a thermal cycling environment is carried out. A thermal cycling degradation model was proposed by considering outgassing property of nonmetal materials and low-cycle mechanical fatigue of ductile and brittle materials. The effects of thermal cycling on operational stability and dynamic performance of two types of PTRs are investigated rigorously with a combination of numerical analysis and experimental study. The experimental data show good fitting with the thermal cycling degradation model. Finally, a reliability estimation of PTRs was obtained through using the Weibull distribution. The proposed novel methodology enables the cooler manufacturers to more quickly and accurately assess the lifetime and reliability of the space PTRs. The rest of the paper is organized as follows. Section 2 establishes a thermal cycling performance degradation model based on the failure mechanism and thermomechanical characteristics of PTRs. Section 3 systematically designs the experimental program of thermal cycling tests. Section 4 offers the results of the thermal cycling tests and presents the lifetime prediction and reliability estimation methodology and the final results. Section 5 concludes the paper.

2. Thermal Cycling Degradation Model

In order to simulate the flight-like environment, cold-tip temperature and cooling power of the PTRs were almost kept constant to cool the instruments while the input electrical power was periodically varied in response to the heat reject temperature evolution. If the cooling temperature was increased due to performance degradation, input electrical voltage would be increased to maintain cold-tip temperature constant. Therefore, the power consumption evolution could indicate the performance degradation of the PTRs. In this paper, performance degradation of the PTRs is defined as an increase of the initial power consumption to maintain cooling temperature constant during long-term operation.

Generally, typical failure mechanisms, i.e., gaseous contamination, wear, fatigue, and leakage, influence stable and long-term operation of PTRs [16–19]. With the key technology development [20–22], such as flexible bearings, metal O-ring seal, and clearance seal, the adverse effect of wear and leakage has been greatly reduced. Gaseous contamination and fatigue have become the two important factors that still greatly affect the reliable and long-lifetime operation of the PTRs on orbit. Usually, high-purity helium is used as working gas in the PTRs. Gaseous contamination can be referred to the foreign gas that lead to impurity of the working helium gas and thus induce cooling performance loss of the PTRs. The key nonmetal materials which release internal gaseous contamination in the PTR mainly include motor glue and piston bushing in the compressor and outer shell in the regenerator. Our engineering experience and previous investigation [14–16] have shown that thermal cycling is mainly responsible for the instability operation of PTRs. The repeated varying heat reject temperature and cyclic power consumption will cause thermal expansion and contraction between the cylinder and the piston of compressor which may induce thermomechanical stresses and induce released contaminants blockage in the regenerator or heat exchanger.

The factors that influence the cooling performance of PTRs are the number of thermal cycle and cycle frequency, heat reject temperature difference, and maximum heat reject temperature. The functional form of the thermal cycling degradation model can be expressed as

$$P_{\text{loss}} = f\left(N, \Delta T, f, T_{\max}\right), \tag{1}$$

where N is the cycle number, ΔT is heat reject temperature difference, f is the cycle frequency, and $T_{\max}$ is the maximum heat reject temperature.

Due to lack of failure life data of PTRs, most manufacturers cannot provide enough lifetime information. The degradation model of PTRs should reflect the two failure mechanisms as contamination and fatigue induced by thermal cycling. Previous studies [23, 24] reported that the outgassing property of nonmetal materials has an exponential function relationship with ambient temperature and operation time as follows:

$$m = m_0 \exp\left(BT\right)\left[1 - \exp\left(\frac{-t}{A}\right)\right], \tag{2}$$

where m_0 is the initial contamination level, B is the temperature dependent coefficient, T is the reject temperature; t is the operation time; and A is the time dependent constant.

With respect to the influence of reject temperature fluctuation and power evolution, low-cycle (few hundred or thousand cycles to produce failure) mechanical fatigue data

for either ductile or brittle materials are effectively modeled using CM model as [25]

$$\Delta D \propto N^c, \tag{3}$$

where ΔD is the performance damage caused by thermal stress, N is the thermal cycle number, and c is the thermal stress coefficient.

Consequently, based on the above outgassing property of nonmetal materials and thermal cycle fatigue model, a theoretical thermal cycling degradation model is established to describe the correlation between power consumption increment of the PTRs and cycle number, reject temperature fluctuation, thermal cycling frequency, and maximum reject temperature based on the following assumptions:

(1) Thermal cycling is the only related factor for performance degradation of the PTRs

(2) The failure mechanism of the PTRs at thermal cycling condition is consistent with that at normal condition

(3) Performance of the PTRs degrades continuously; each thermal cycle causes performance damages

$$P(N, \Delta T, f, T_{\max}) = P_0 + N^{a_1} \cdot \Delta T^{a_2} \cdot f^{a_3} \cdot \exp\left(\frac{\beta}{T_{\max}}\right), \tag{4}$$

where P_0 is the initial power consumption of the PTRs, a_1 is thermal cyclic coefficient, a_2 is the reject temperature difference related parameter that indicates the effect of temperature fluctuation, a_3 is the frequency dependent parameter, and β is the Arrhenius law factor that represents the upper reject temperature effect.

The higher frequency of the thermal cycle will lead to the greater thermal shock and accelerate the performance degradation process of the PTRs. The repeated varying heat reject temperature and cyclic power consumption will cause fatigue of ductile and brittle materials of the PTRs. In this study, the low frequency of the thermal cycle means low temperature change rate (2.08 K/h) and the influence of the thermal shock on the performance of the PTR will be small. Thus, the frequency term can be neglected in the thermal cycling degradation mode. So, equation (4) is reduced to a three-parameter function as follows:

$$P(N, \Delta T, T_{\max}) = P_0 + N^{a_1} \cdot \Delta T^{a_2} \cdot \exp\left(\frac{\beta}{T_{\max}}\right). \tag{5}$$

Then, the nonlinear degradation model (equation (5)) can be linearized in the form of $y = a \cdot x + b$ by taking the logarithm on both sides:

$$\ln(\Delta P) = \ln\left(P(N, \Delta T, T_{\max}) - P_0\right) = a_1 \ln N + a_2 \ln \Delta T + \beta \frac{1}{T_{\max}}, \tag{6}$$

$$y = a_1 \cdot x + k_1 \cdot a_2 + k_2 \cdot \beta,$$

where $y = \ln(\Delta P)$, $x = \ln N$, $k_1 = \ln \Delta T = \ln(283 - 273) = 3.6889$, $k_2 = 1/T_{\max} = 0.0035$, and a_1, a_2, and β are the unknown model parameters.

3. Experiment Design and Procedure

3.1. Specimen Preparation. According to the mission requirements, two types of pulse tube refrigerators with required cooling capacity of 1W@60 K with maximum input electrical power of 80 W (type A) and 5W@80 K with maximum input electrical power of 120 W (type B) have been developed and provided in the test. The experimental specimens have undergone a verification testing to verify the thermal performance before carrying out the thermal cycling test. A schematic diagram of the pulse tube refrigerator is shown in Figure 1, and a photograph of the prototypes is depicted in Figure 2. The PTRs mainly consist of a dual-piston linear compressor, a regenerator, a pulse tube, a gas reservoir, and heat exchangers at cold and hot ends. The prototype PTRs operate at frequency of 50 Hz with the working gas He at an average pressure of 3.25 MPa. The basic specifications of the PTRs are described in Table 1.

3.2. Testing Profile. In our preliminary test, the PTR has the capability to successfully work after experiencing the extreme nonoperational temperature range from 223 K to 323 K. To demonstrate the capability at operational conditions, the PTRs were needed to continuous operate at the simulated space environment. Therefore, the testing profile of the thermal cycling test was designed and defined as depicted in Figure 3 to simulate the space environment and verify the thermal stability and long lifetime of the PTRs. The parameters of testing profile of the PTRs, such as dwell time, ramp rate, and temperature extremes, were given according to the requirement of temperature control and typical operating conditions in orbit. The heat reject temperature range of the PTRs was approximately from 243 K to 283 K, and one cycle time from low temperature to high temperature was about 168 h. Each cycle included a 60 h dwelling time at lower or upper temperature and 24 h for ramping up time or cooling down time as shown in Figure 3. Details of thermal cycling test profile of the PTRs are listed in Table 2.

3.3. Experimental Apparatus. Figure 4 shows a detailed schematic of the test setup. The experimental apparatus mainly consisted of data measuring facility, data saving facility, data monitoring facility, and thermal control system. The prototypes were installed in cylinder vacuum chambers (Figure 4(c)) to simulate the temperature and vacuum environment in orbit. The interesting performance parameters of the PTRs mainly included cold-tip temperature, input electrical power, heat rejection temperature, and heating load. Linear compressors of the pulse tube cryocoolers were driven by AC power sources with an accuracy of ±0.01 W. The cold-tip temperature and heat reject temperature at the hot end of the prototypes were measured via calibrated platinum (Pt100) resistance thermometers with an accuracy of ±0.1 K. The heaters with heating power of 1 W (type A)

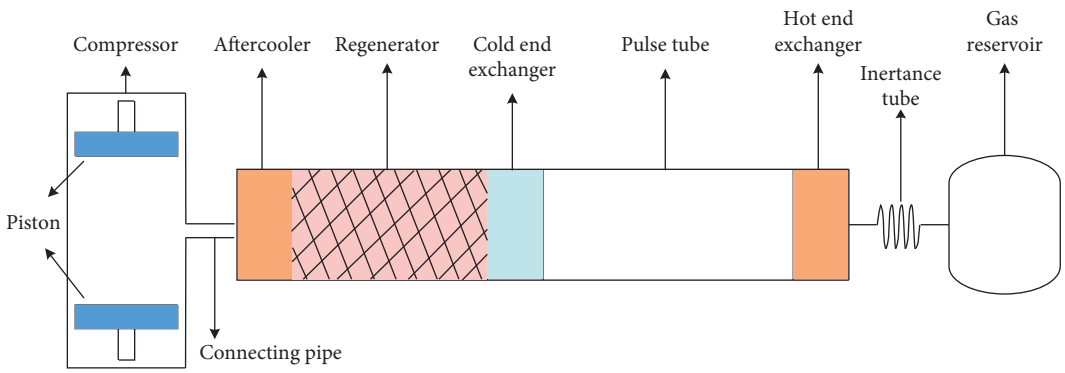

Figure 1: Schematic diagram of the pulse tube refrigerator.

(a) (b)

Figure 2: Prototypes provided for the thermal cycling test. (a) Type A pulse tube cryocooler. (b) Type B pulse tube cryocooler.

Table 1: Basic specification of the PTRs.

Parameter	Value	
	Type A	Type B
Cooling capacity	1 W at 60 K	5 W at 80 K
Total mass	7.5 kg	8.2 kg
Operational frequency	50 Hz	50 Hz
Maximum power consumption	80 W	120 W
Configuration	Single stage	Single stage
Pressure of helium gas	3.25 MPa	3.25 MPa
Designed lifetime	8 years	8 years
Sample size	2	2
Reject temperature		
Nonoperation	223–323 K	223–323 K
Operation	243–283 K	243–283 K

and 5 W (type B) via DC power supplies with an accuracy of ±0.01 W were applied to the cold heads to balance the cooling power. The cooling components such as heat plate and heat pipes (Figure 4(a)) were applied to control heat rejection temperature though transporting waste heat from the heat exchanger (Figure 4(b)) to a radiator and then rejected to outer space. The NI-LabVIEW-based data acquisition module and operation control unit (Figure 4(d)) were developed for saving and monitoring and controlling operational conditions of pulse tube cryocoolers in real-time. The control unit adjusted the motor motion of linear compressor to maintain the required cold-tip temperature, and it also provided power supplies, temperature control, and failure protection during thermal cycling tests. The

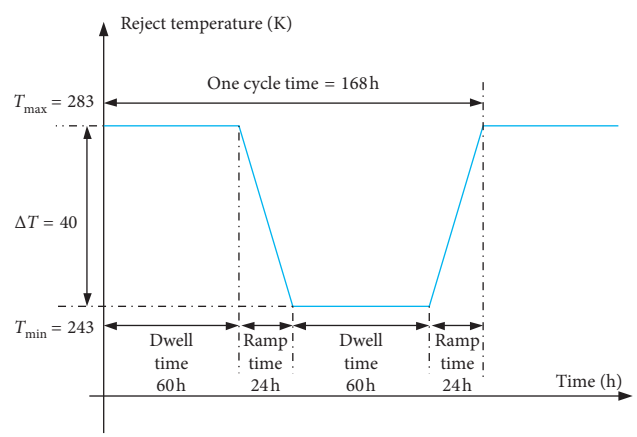

Figure 3: Schematic of testing profile for the thermal cycling test.

Table 2: Details of the thermal cycling test profile.

Parameters	Values
Heat reject temperature range (K)	243–283
Dwell time (h)	60
Ramp time (h)	24
Ramp rate (K/h)	2.08
One cycle time (h)	168
Test status	Continuous operation

control unit based on the PID (proportion integration differentiation) control algorithm is widely used in the cold-tip temperature control of the PTRs. By controlling and

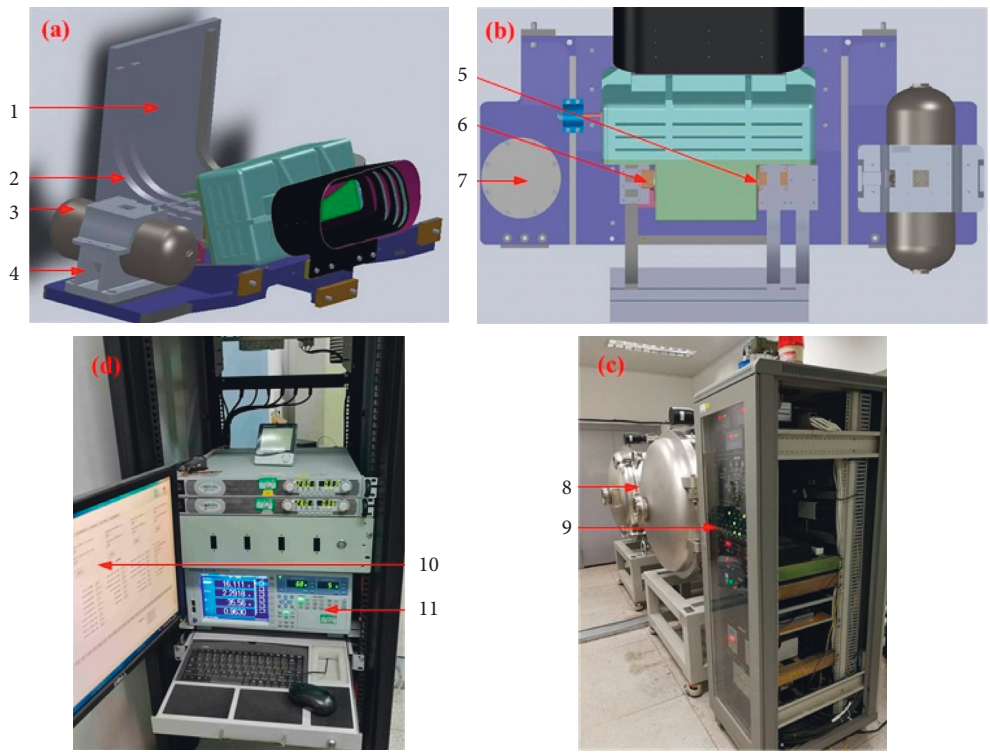

Figure 4: Experimental facilities. (1) Heat plate; (2) heat pipe; (3) linear compressor; (4) base of the compressor; (5) after cooler; (6) hot end heat exchanger; (7) reservoir; (8) two vacuum chambers; (9) data acquisition modules; (10) data acquisition software; (11) input power supply.

Table 3: Failure criterion of PTRs.

Prototype	Performance parameter	Case 1	Case 2	Case 3
Type A PTR	Input power increment (W)	$\Delta P \leq 10$	$10 < \Delta P \leq 25$	$\Delta P > 25$
	Cold-tip temperature difference (K)	$\Delta T \leq 3$	$3 < \Delta T \leq 5$	$\Delta T > 5$
	Conclusion	Operates well	Degradation	Failure
Type B PTR	Input power increment (W)	$\Delta P \leq 10$	$10 < \Delta P \leq 20$	$\Delta P > 20$ or
	Cold-tip temperature difference (K)	$\Delta T \leq 3$	$3 < \Delta T \leq 5$	$\Delta T > 5$
	Conclusion	Operates well	Degradation	Failure

calculating the difference between the set and measured temperature, the driving input electrical voltage of the PTRs is adjusted, so that the cold-tip temperature of the PTRs can be kept stable.

3.4. Failure Criterion. The lifetime requirement of the PTRs is achieved at least after 8 years continuous operation in orbit. The cooling capacity of type A PTR is required to provide cooling power of 1 W with stable cold-tip temperature of 60 K, and the type B PTR is required to provide cooling power of 5 W with cold-tip temperature of 80 K. As the PTRs have to provide sufficient cooling for the science instruments and optical system as well as to meet the 8 years lifetime requirement, the failure criterion of pulse tube refrigerator is mainly determined by the power consumption increment and the cold-tip temperature. During the thermal testing, a PTR is considered as performance degradation or failure if it could not meet the criteria which are specifically declared in Table 3.

4. Results and Discussion

4.1. Experimental Results. Two years of thermal cycling tests have been completed from August 2016 to September 2018 for about 100 cycles to assure adequate thermomechanical stability and demonstrate long lifetime and high reliability of the type A and type B PTRs. Two type A prototypes and two type B prototypes have been prepared and tested for about 18000 hours. The experimental results are obtained as shown in Figures 5 and 6 and are summarized in Table 4. As these experimental data have been filtered to eliminate off abnormal conditions such as shutdown or restart, the effective testing time is about 16000 hours. In addition, leakage tests of the prototypes have been performed before and after the thermal cycling tests and the leakage rates of the whole machine are about 3×10^{-8} Pa·m^3/s, which meet the required leakage rate ($<1.0 \times 10^{-7}$ Pa·m^3/s).

Figure 5 shows the results of power consumption variations (left axis) and cold-tip temperature evolution (right axis) as a function of time. As depicted in Figures 5(a) and 5(b),

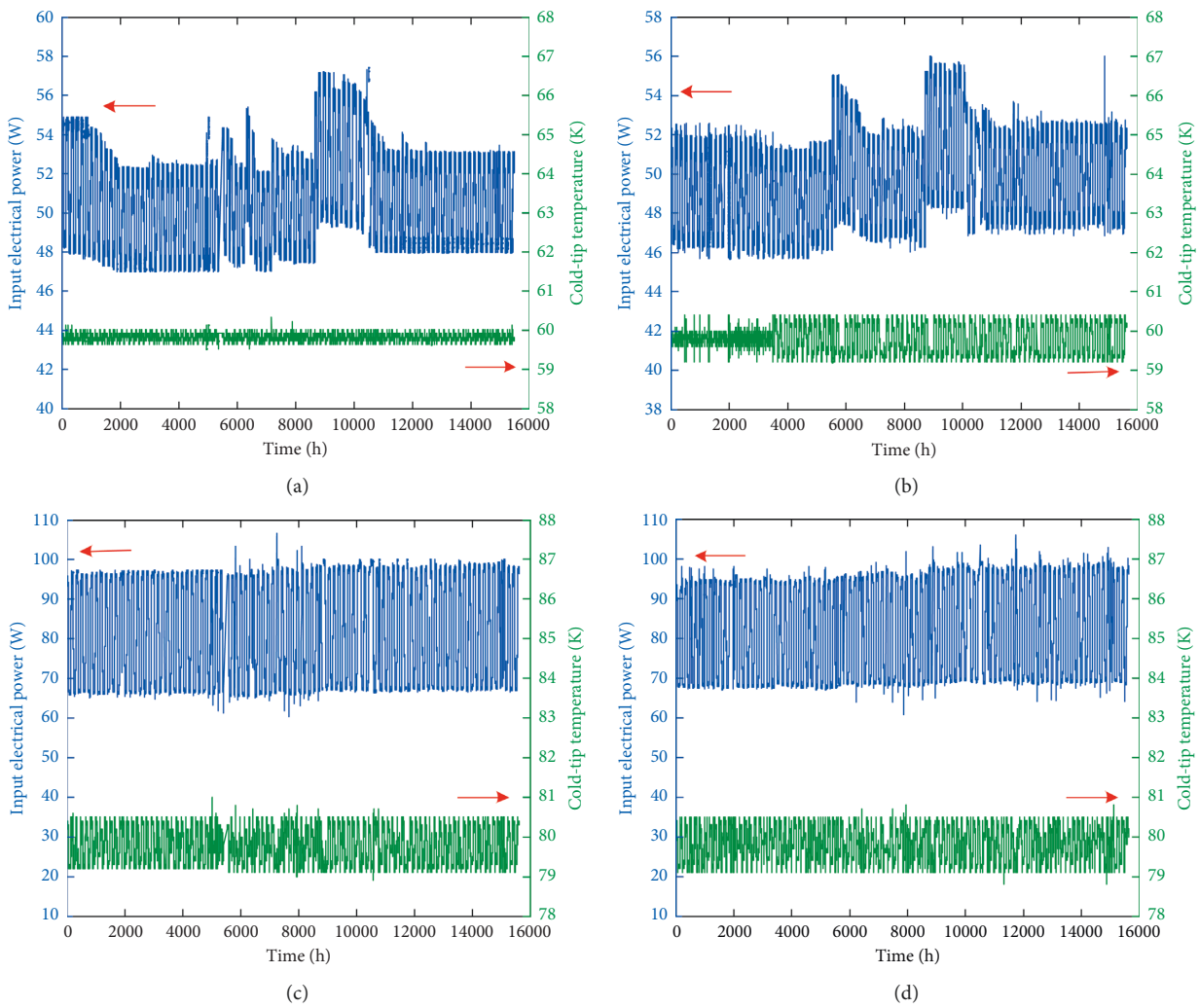

Figure 5: Operation status of the PTRs in the thermal cycling test: (a, b) 1 W@60 K PTR; (c, d) 5 W@80 K PTR.

cold-tip temperatures of type A prototypes could reach and operate stably at 60 ± 0.6 K with the input electrical power at range of 45–60 W. The main reason for the increase of cold-tip temperature fluctuation of type A No. 2 after operation 4000 h is the instability of control unit of the PTRs under complex working conditions. Similarly, the cold-tip temperature of type B prototypes could reach and maintain the preset point of 80 K with fluctuation less than 0.7 K with 64–100 W input electrical power. Therefore, the cooling capacity of both type A and type B prototypes was satisfied the requirements for space applications as listed in Table 3 of Section 3.4.

Figure 6 shows the effect of repeated varied heat rejection temperature on the power consumption of the PTRs when the heating power and cold-tip temperature are maintained at constant. As depicted in these figures, power consumptions of four prototypes are cyclic increased and decreased as reject temperature increases from 243 K to 283 K. The curves of power consumption evolution follow a similar variation trend with the heat rejection temperature in a cycle, which indicate that the cooling capacity of PTRs was significantly influenced by the reject temperature variation. For instance, in the 10th thermal cycle as shown in Figure 7, the input electrical power of type A No. 1 prototype increased from 47.32 W to 53.23 W when the reject temperature increased from 243 K to 283 K. The increasing slope is around 1.48 W/10 K. Similarly, the increasing slop of type A No. 2 and type B No. 1 and No. 2 are 1.35 W/10 K, 7.58 W/10 K, and 6.78 W/10 K, respectively.

4.2. Operational Characteristics under Thermal Cycling

4.2.1. Thermal Stability Performance. The increasing modern space-borne cryogenic detectors have driven the demands for higher thermal stability to obtain high quality of signal and image. Thermal stability is an important indicator to verify the high reliability and long lifetime of PTRs. At thermal cycling condition, the period of cool-down, restabilization, and heating up has adverse impact on thermal stability of PTRs. A PTR should maintain its thermal performance even if it is subjected to thermal cycling environment. In this sense, changes in cold-tip temperature and power consumption were investigated and determined after thermal cycling tests.

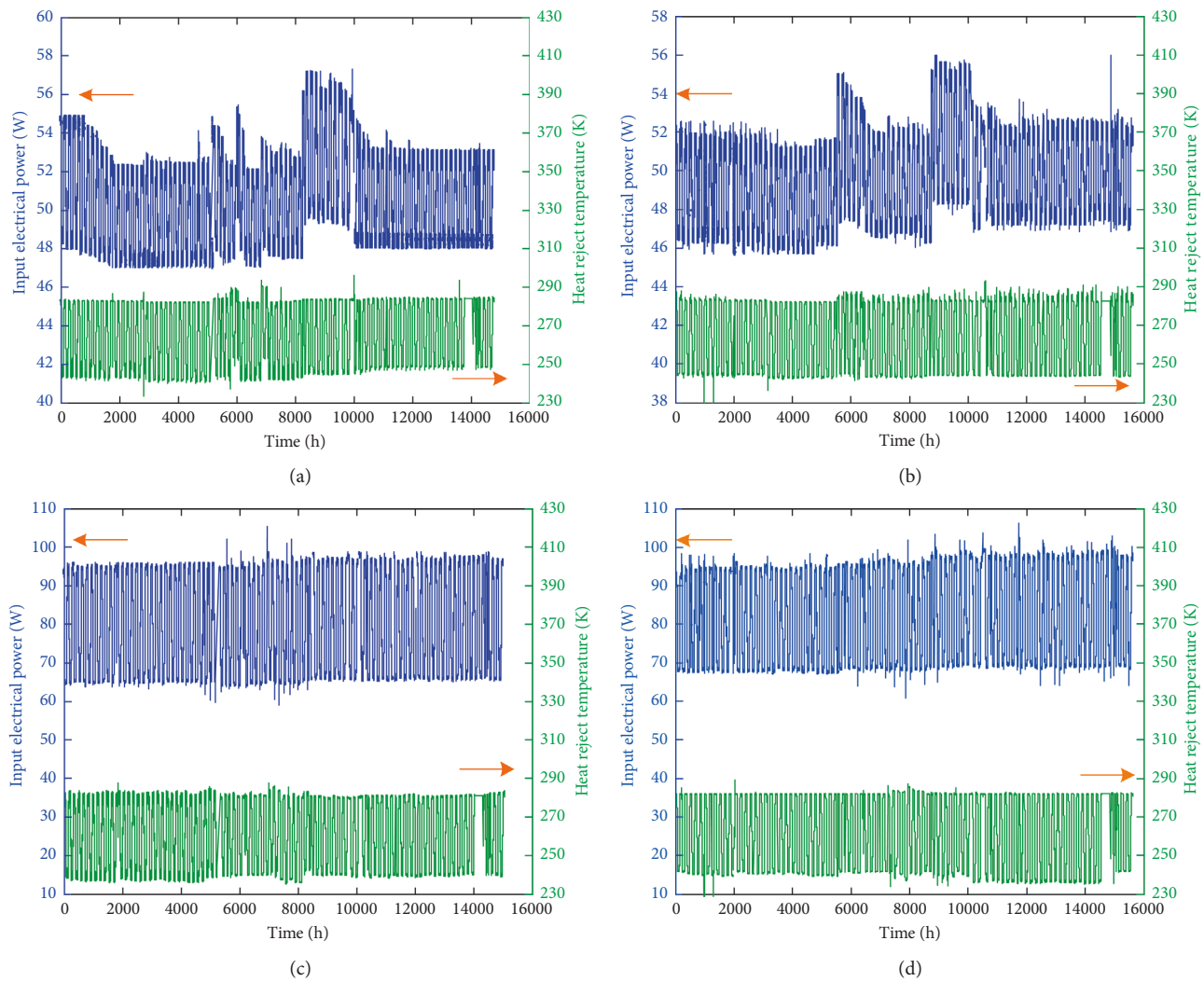

Figure 6: Effect of reject temperature cycle on cooling performance of the prototypes with constant heat power and cooling temperature: (a, b) 1 W@60 K PTR; (c, d) 5 W@80 K PTR.

Table 4: Summary of thermal cycling test results.

Prototype	Sample	Testing Time (h)	Heat reject temperature (K)		Cold-tip temperature (K)		Input electrical power (W)	
			Preset value	Result	Requirement	Result	Requirement	Result
Type A	No. 1	16000	243~283	241.1~283.2	≤63	60 ± 0.2	$P \leq 80$	47.02~56.21
	No. 2	16000	243~283	242.9~282.7		60 ± 0.6		45.73~54.62
Type B	No. 1	16000	243~283	241.8~286.4	≤83	80 ± 0.7	$P \leq 120$	64.95~97.31
	No. 2	16000	243~283	240.2~283.7		80 ± 0.6		67.56~96.73

The mission requirement of long-term and short-term (one cycle) cold-tip temperature stability of the PTRs is to keep the detectors at a specified cryogenic temperature with fluctuation less than 3 K and 1 K, respectively. Figures 8 and 9 illustrate the capability for the short-term and long-term stability of the PTRs with heat reject temperature varying from 243 K to 283 K. A small cold-tip temperature difference (0.2 K–0.8 K) was observed as shown in Figure 8. It can be seen from Figure 9 that the cycle-averaged cold-tip temperatures remain stable during 16000 h operation within ±1 K of the set points of 60 K for type A prototypes and 80 K for type B prototypes, respectively, which reach the requirement of temperature fluctuation (<3 K).

Furthermore, the average power consumption at upper reject temperature is adopted to indicate the performance instability or degradation of the PTRs. These data can be obtained from the test results in Section 4.1 and are presented in Figure 10. The figures depict the average power consumption of the prototypes as a function of cycle number. On one hand, as shown in Figure 10(a), the average power consumption of samples No. 1 and No. 2 of type A PTRs gradually decreases at the initial stage and tends to be

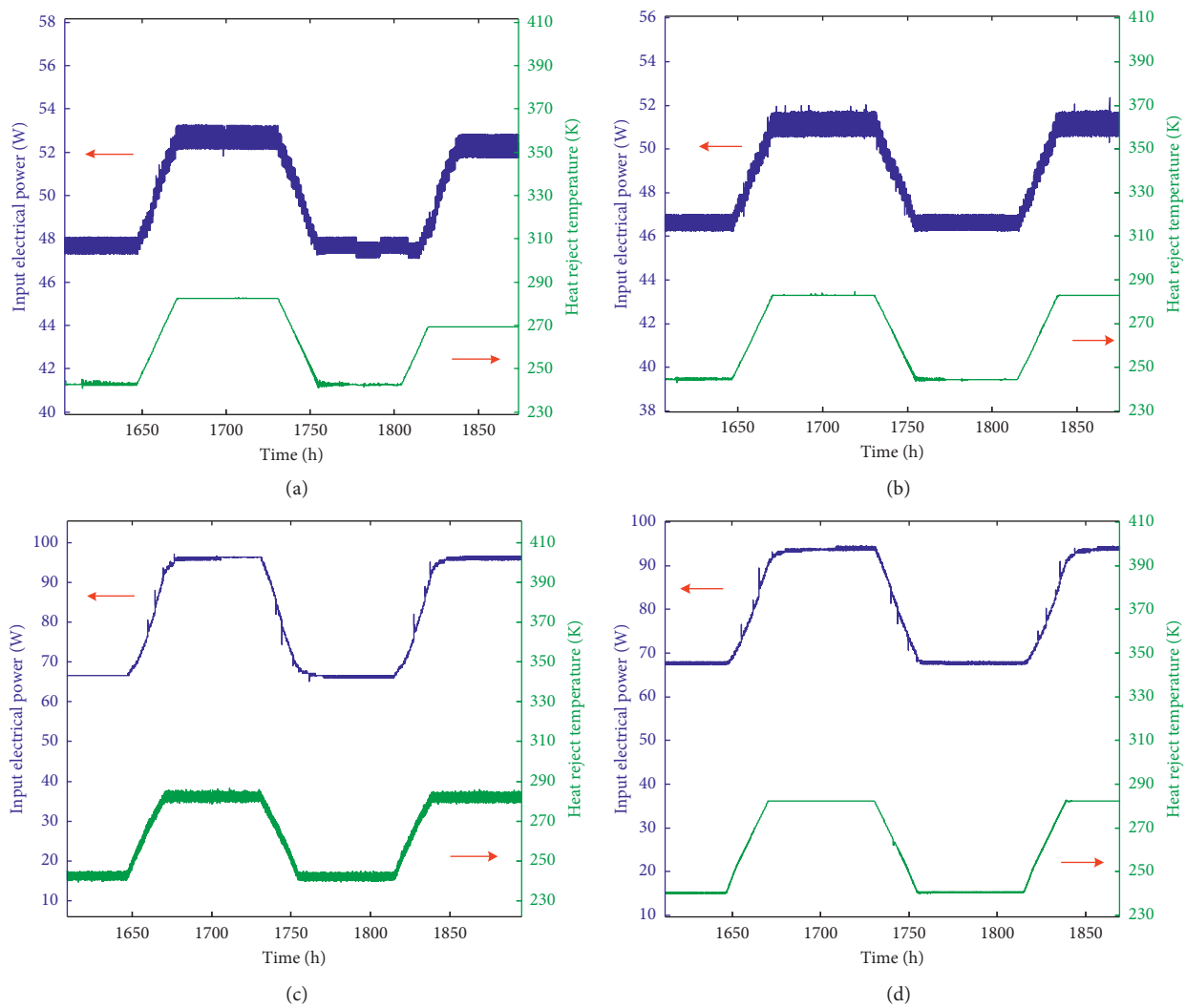

Figure 7: Dependence of PTR performance on the heat reject temperature: (a, b) 1 W@60 K PTR; (c, d) 5 W@80 K PTR.

stable during later stages of the thermal cycling tests, and the maximum power difference is 3.83 W for type A prototype, when sample No. 1 drops from 54.62 W to 51.79 W at the initial stage. On the other hand, Figure 10(b) shows that the type B prototypes operate with a power fluctuation at the most of operational time and performance degradation has occurred at the end of the thermal cycling test. It also can be seen from Figure 10(b) that the initial power fluctuation of type B prototypes is 1.73 W when the average power consumption of sample No. 1 increases from 95.25 W to 96.98 W. Therefore, the power consumption of type A and type B prototypes can remain in a reasonable range in response to the reject temperature change. Based on the results above, the thermal adaptability and stability of type A and type B PTRs are both successfully verified under thermal cycling condition.

Figure 10 also shows the type A and type B prototypes restarted operation after accident shutdown at points A–D. It is particularly important to note that the power consumption of type A PTRs gradually drops like the cool-down process after restarting operation at a period of time, which shows that the cooling capacity is almost completely recovered compared to the previous status. The above typical phenomenon indicts the performance degradation of type A PTRs happened most likely causing by gaseous contamination. Some condensable gas contaminants such as water vapor or carbon dioxide will gradually freeze and be absorbed on cold surfaces at low temperatures condition, especially in the regenerator which is made of porous materials, which will increase flow resistance and heat conduction and block passage of regenerator, thus leading to performance degradation of the PTRs. The effect of gaseous contamination on the performance degradation of the PTRs is apparently different from the mechanical failure modes: performance degradation caused by gas contamination could restore mostly to the original performance when the PTRs restart running after having been turned off for a period of time; however, the mechanical failure modes do not have this feature.

4.2.2. Dynamic Performance of PTRs. In order to determine the dynamic performance of the investigated PTRs, the

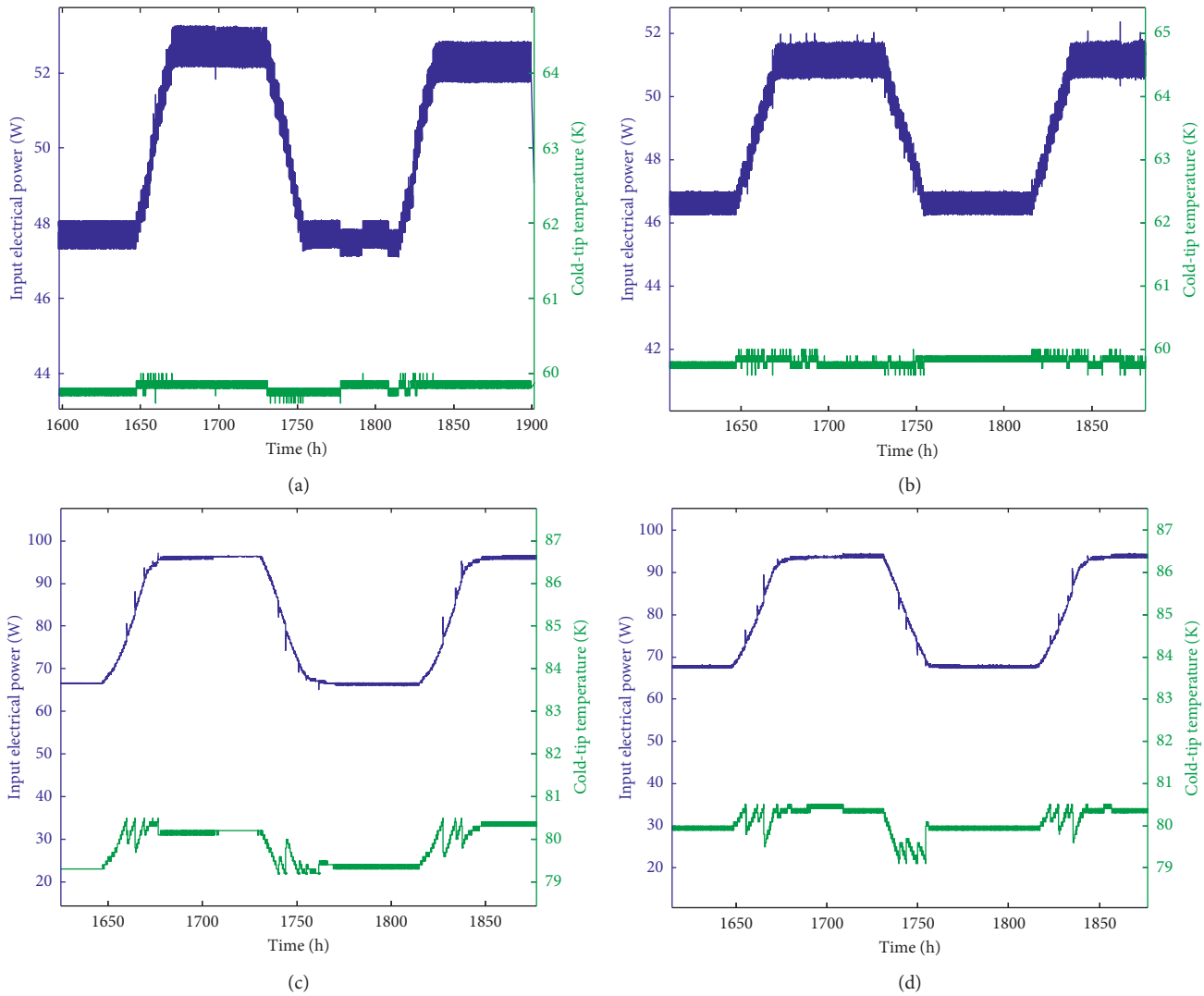

Figure 8: Short-term stability of cold head temperature in the 10th reject temperature cycle: (a, b) type A PTRs; (c, d) type B PTRs.

cooling capacity parameters, such as COP (coefficient of performance) and relative Carnot efficiency under thermal cycling condition are used and calculated as equations (7) and (8), and the results are presented in Figures 11 and 12.

$$\mathrm{COP}_i = \frac{Q_C}{W_{\mathrm{ave}}}, \tag{7}$$

$$\eta_{\mathrm{Carnot}} = \frac{Q_c}{W_{\mathrm{ave}}} \times \frac{T_a - T_m}{T_m} \times 100\%, \tag{8}$$

where Q_C is the cooling power, W_{ave} is average power consumption of the PTRs at upper or lower heat reject temperature condition, T_m is the mean cooling temperature of the PTRs, and T_a is the heat reject temperature of the PTRs.

Figures 11 and 12 present the efficiency of the type A and type B PTRs operating at upper or lower heat reject temperature conditions. It is obvious that COP and relative Carnot efficiency has a similar variation trend as the function of temperature cycle. As depicted in Figure 11, the relative Carnot efficiency at lower heat reject temperature is better than that of at upper heat reject temperature. This is probably due to the greater heat losses induced by larger temperature difference at the upper heat reject temperature condition. At lower heat reject temperature condition, the No. 1 and No. 2 type A PTRs with cooling power of 1 W at 60 K can achieve the mean relative Carnot efficiency of 7.8% and 8.1%, respectively; the No. 1 and No. 2 of type B PTRs can achieve higher mean relative Carnot efficiency of 15.6% and 15.1%, respectively. Figure 12 shows the dynamic COP of the PTRs. As these figures illustrated, the maximum COP of the type A and type B PTRs is about 2.1% and 7.5%, respectively. From the results above, it is revealed that the type B PTR has a better dynamic thermal capability than type A PTR to achieve high efficiency.

4.3. Lifetime Estimation Methodology and Results. As the performance degradation of the PTRs did not reach the preset failure criterion, the actual failure lifetime of the PTRs could not be obtained during thermal cycling tests. Therefore, the pseudo-failure lifetime (Figure 13) instead of the

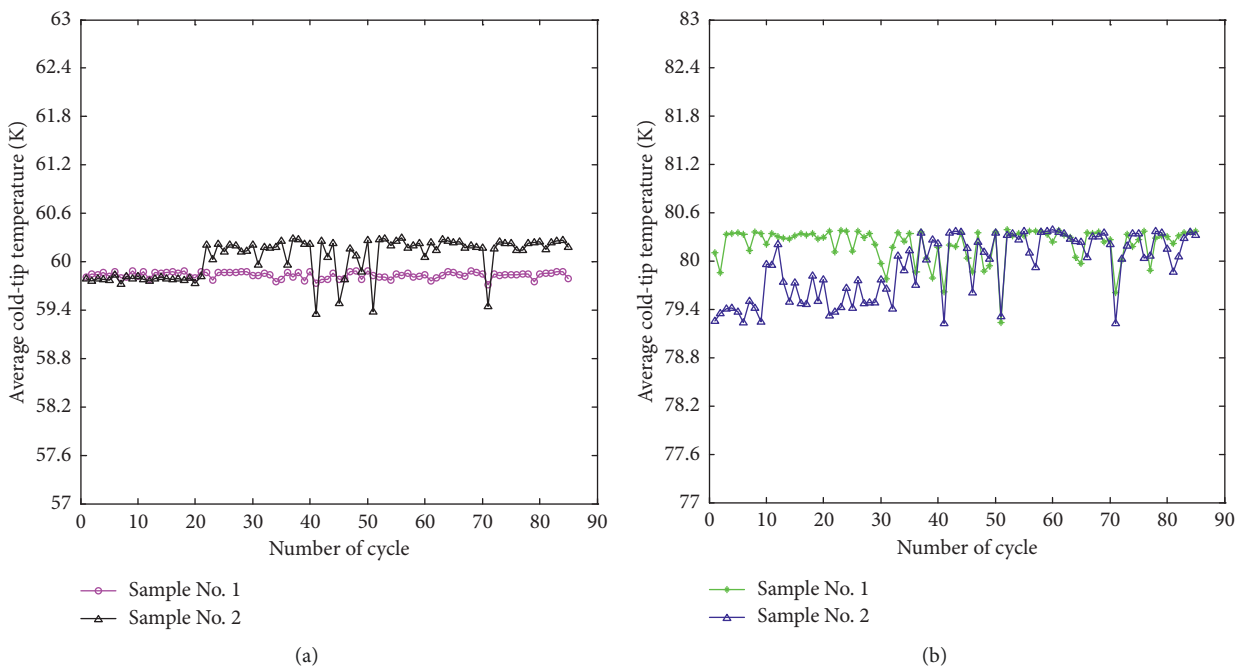

Figure 9: Long-term stability of cold head temperature for 16000 h operation: (a) type A; (b) type B.

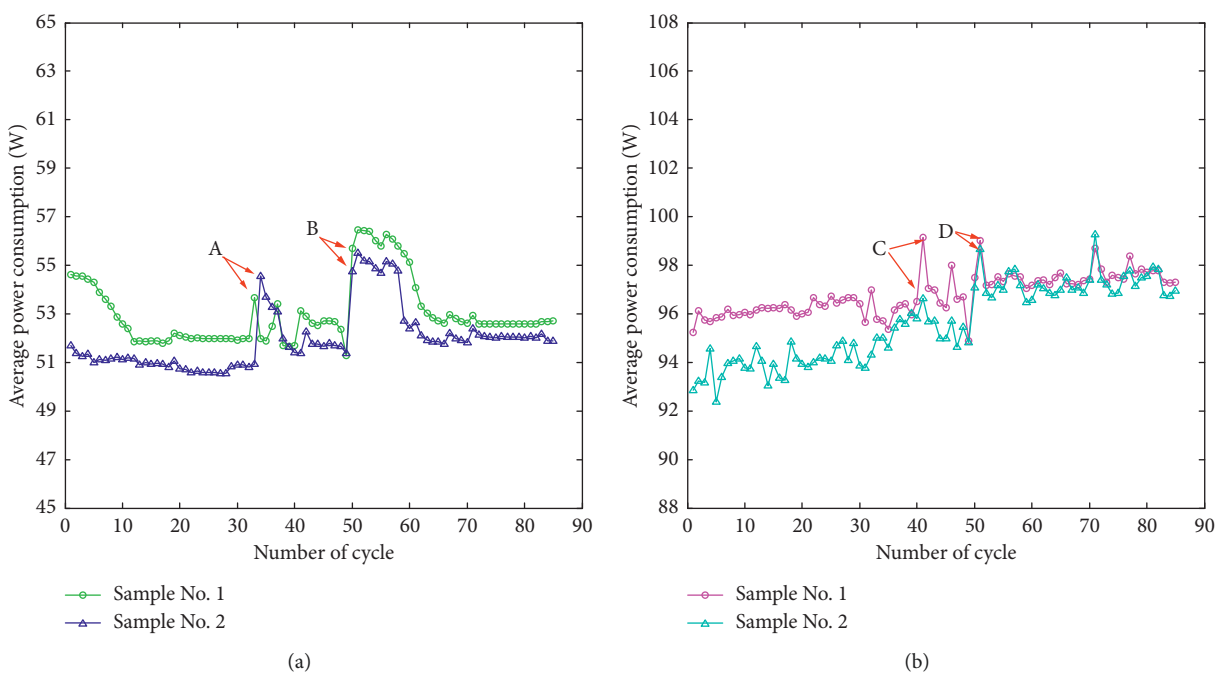

Figure 10: Average power consumption of the PTRs versus number of thermal cycle: (a) type A prototypes; (b) type B prototypes.

real failure lifetime was adopted to predict the operational lifetime and to estimate the reliability of the PTRs [26, 27]. The basic idea of the statistical analysis of performance degradation data of PTRs based on pseudo-failure lifetime is through the following four steps.

Step 1. Establish a performance degradation model based on the failure mechanism of the PTRs and use experimental data (t_i, N_i, P_i) of the ith sample to describe the performance degradation curve of the ith sample:

$$P_i = f\left(N, \Delta T, f, T_{\max}; a_{1i}, a_{2i}, \beta_i\right). \tag{9}$$

Step 2. Estimate the parameters $(a_{1i}, a_{2i}, \beta_i)$ of performance degradation curve of each sample by least square method or nonlinear least square method based on measured

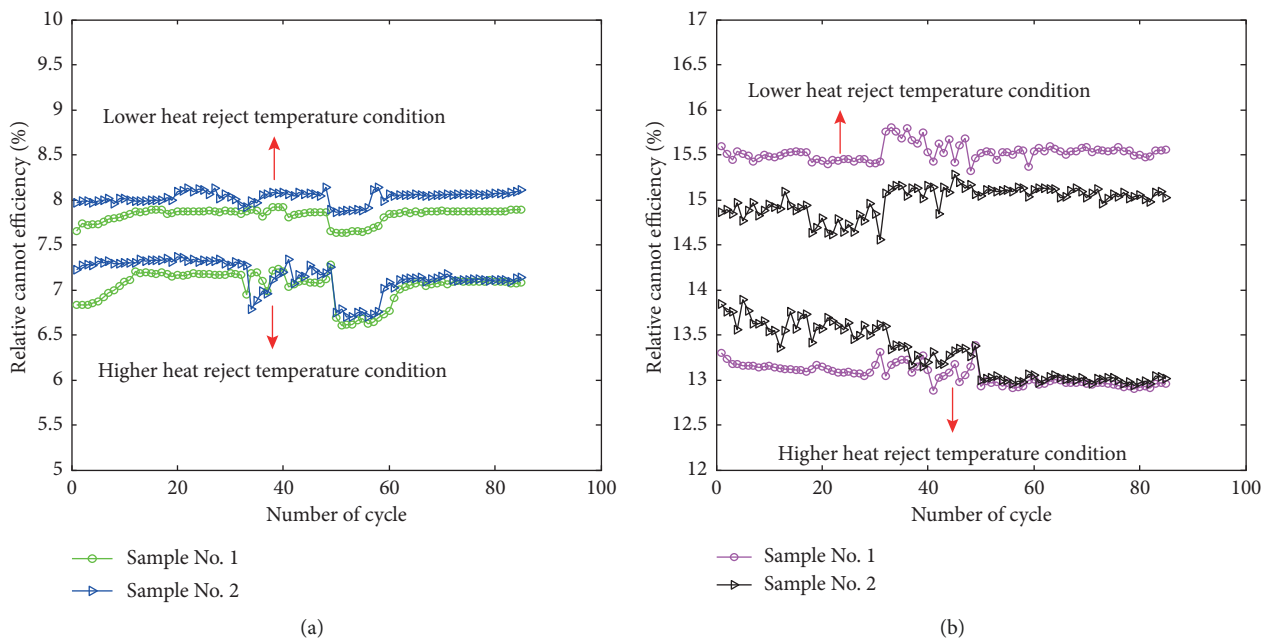

Figure 11: Relative Carnot efficiency of PTRs depending on the thermal cycle: (a) type A; (b) type B.

performance degradation data (t_j, N_j, P_{ij}), ($i = 1, 2, \ldots, n$; $j = 1, 2, \ldots, m$):

$$P_i = f\left(N, \Delta T, f, T_{\max}; \widehat{a}_{1i}, \widehat{a}_{2i}, \widehat{\beta}_i\right), \tag{10}$$

where i is the number of the test samples ($i = 1, 2, \ldots, n$), j is the record time of the test samples ($j = 1, 2, \ldots, m$), and $\widehat{a}_{1i}, \widehat{a}_{2i}$, and $\widehat{\beta}_i$ are the estimated parameter values of the performance degradation model.

Step 3. Obtain the pseudo-failure life $(\widehat{N}_1, \widehat{N}_2, \ldots, \widehat{N}_i)$ through the degradation model and the failure threshold D_f.

$$N_i = f^{-1}\left(D_f, \Delta T, f, T_{\max}; \widehat{a}_{1i}, \widehat{a}_{2i}, \widehat{\beta}_i\right), \tag{11}$$

where f^{-1} is the inverse function of f in equation (10).

Step 4. Using the estimated pseudo-failure lifetime $(\widehat{N}_1, \widehat{N}_2, \ldots, \widehat{N}_i)$ to find the lifetime failure distribution function $F(t)$ of the PTRs. Moreover, check the goodness of fit of the failure lifetime distribution.

4.3.1. Estimated Model Parameter Values. The average power consumption data of the PTRs at upper heat rejection temperature were utilized as the thermal cycling degradation data after eliminating off abnormal conditions (as shown points A and B in Figure 10(a)). The experimental data are presented in magenta curves in Figure 14. The nonlinear least square method in MATLAB was adopted to obtain the model parameters values based on multivariate nonlinear degradation model in equation (11) and the degradation data. The results are listed in Table 5, and the fitting data are presented in Figure 14. These pictures illustrate an excellent fitting situation following the tendency of cooling performance degradation of the prototypes No. 1 and No. 2. The fitted curves validate that the proposed degradation model fit the performance degradation of PTRs well under simulated thermal cycling environment. Therefore, this model could be used to predict or evaluate the lifetime of the PTRs.

4.3.2. The Estimated Pseudo-Failure Lifetime. The performance degradation models are established via the estimated model parameters as shown in the following equations with the type A No. 1, No. 2 and type B No. 1, No. 2, respectively:

$$P_{A1} = 48.25 + N^{0.2673} \cdot \Delta T^{0.0830} \cdot \exp\left(\frac{76.2335}{T_{\max}}\right), \tag{12}$$

$$P_{A2} = 47.34 + N^{0.2656} \cdot \Delta T^{0.0798} \cdot \exp\left(\frac{83.2887}{T_{\max}}\right), \tag{13}$$

$$P_{B1} = 92.29 + N^{0.2639} \cdot \Delta T^{0.0778} \cdot \exp\left(\frac{71.2825}{T_{\max}}\right), \tag{14}$$

$$P_{B2} = 91.06 + N^{0.2716} \cdot \Delta T^{0.0756} \cdot \exp\left(\frac{68.9857}{T_{\max}}\right). \tag{15}$$

According to the performance degradation curves and the given failure criterion as presented in Section 3.4 (power consumption increment <10 W), a PTR has a certain lifetime in terms of operation thermal cycles. Since the performance degradation of the PTRs does not reach the failure criterion in the thermal cycling test, real lifetime failure data of the PTRs cannot be obtained. Therefore, the estimated failure lifetimes instead of actual failure lifetimes are acquired as presented in Table 6.

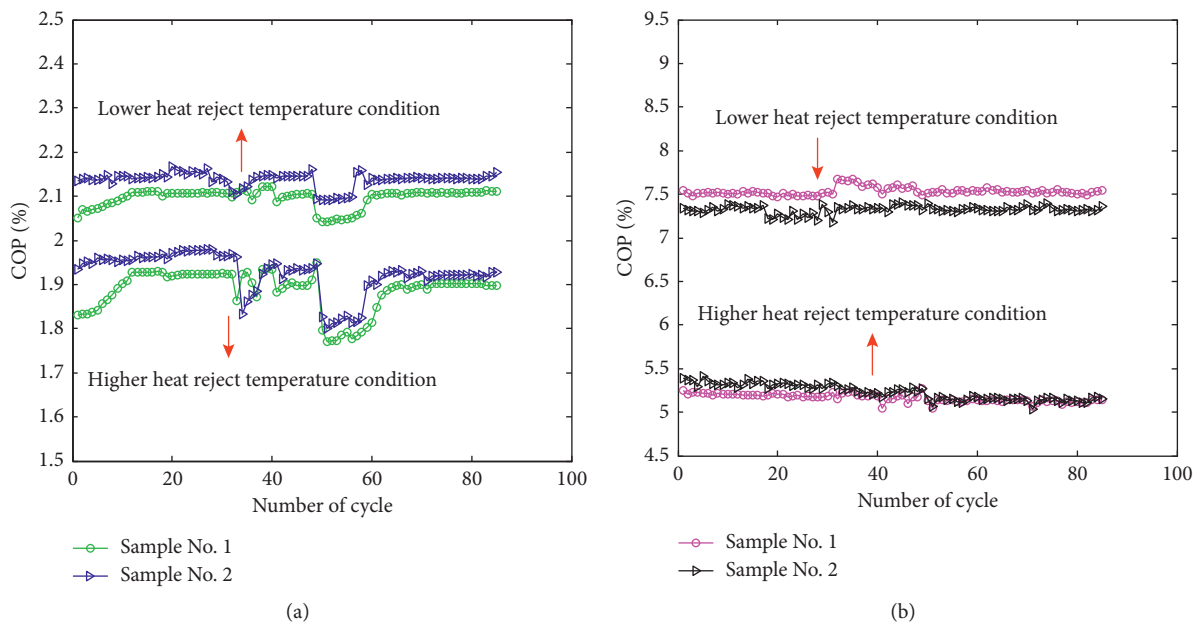

Figure 12: The dynamic COP vs. thermal cycle: (a) type A; (b) type B.

4.4. Reliability Estimation Methodology and Results

4.4.1. Life Distribution and Goodness-of-Fit Test. The failure time data of the PTRs are commonly described by a two-parameter Weibull distribution, which was widely applied by the previous studies [28, 29]. It appears to be a reasonable and accepted method for integral PTRs, which are subjected to performance degradation due to the contamination and fatigue failure mode. The general equation for the cumulative distribution function (CDF) of the Weibull distribution is

$$F(t) = 1 - e^{-(t/\eta)^m}, \tag{16}$$

where m is the shape parameter and it can represent the characteristic life of the product and η is the scale parameter and it is closely related to the stress level at which the product operates: the greater the stress level, the smaller the scale parameter. Based on the results of the estimated failure lifetimes shown in Table 6, the value of the shape parameter $m = 4.5$ was obtained according to the Weibull distribution.

The lower confidence limit of the reliability of the PTRs based on the Weibull distribution can be expressed as

$$R_L = \exp\left[-\frac{t^m}{2t^*}\chi^2_\gamma(2r+2)\right], \tag{17}$$

where

$$t^* = \sum_{i=1}^{n} t_i^m, \qquad \hat{\eta} = \left(\frac{t^*}{r}\right)^{(1/m)}, \tag{18}$$

where t_i $(i = 1, 2, 3, 4)$ is the estimated failure lifetime and the results are shown in Table 6, n is the total numbers of testing prototypes, and r is the estimated failure numbers; therefore, we can obtain $t^* = 3.2 \times 10^{23}$ h and $\hat{\eta} = 122775$ h.

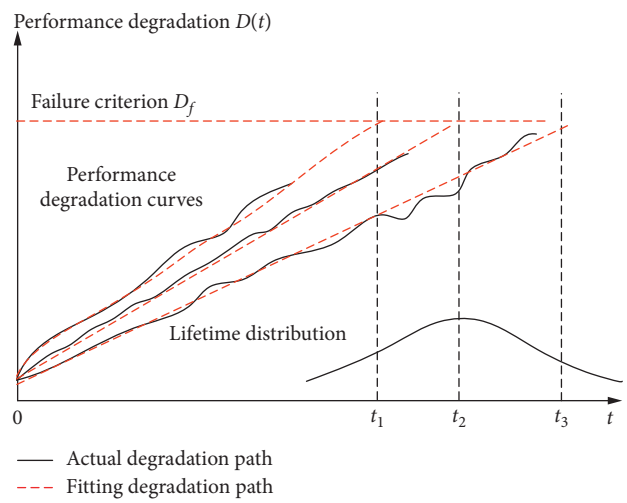

Figure 13: The pseudo-failure lifetime.

The methods for estimating the Weibull parameters are based on the null hypothesis (H_0) that the failure lifetime data follow a Weibull distribution. The goodness-of-fit test is used to evaluate whether H_0 needs to be rejected or accepted, which will indicate that the Weibull distribution provide a good fit to the failure lifetime data under consideration. A significance level $\alpha = 0.05$ is chosen to the statistical analysis, and it defines the confidence level that the data do not follow a Weibull distribution.

There are various goodness-of-fit test methods (Kolmogorov–Smirnov, Cramer–von Mises, chi-squared, etc.) based on the empirical distribution function (EDF) statistics [30]. Among them, the K-S (Kolmogorov–Smirnov) test method has the advantages of being suitable

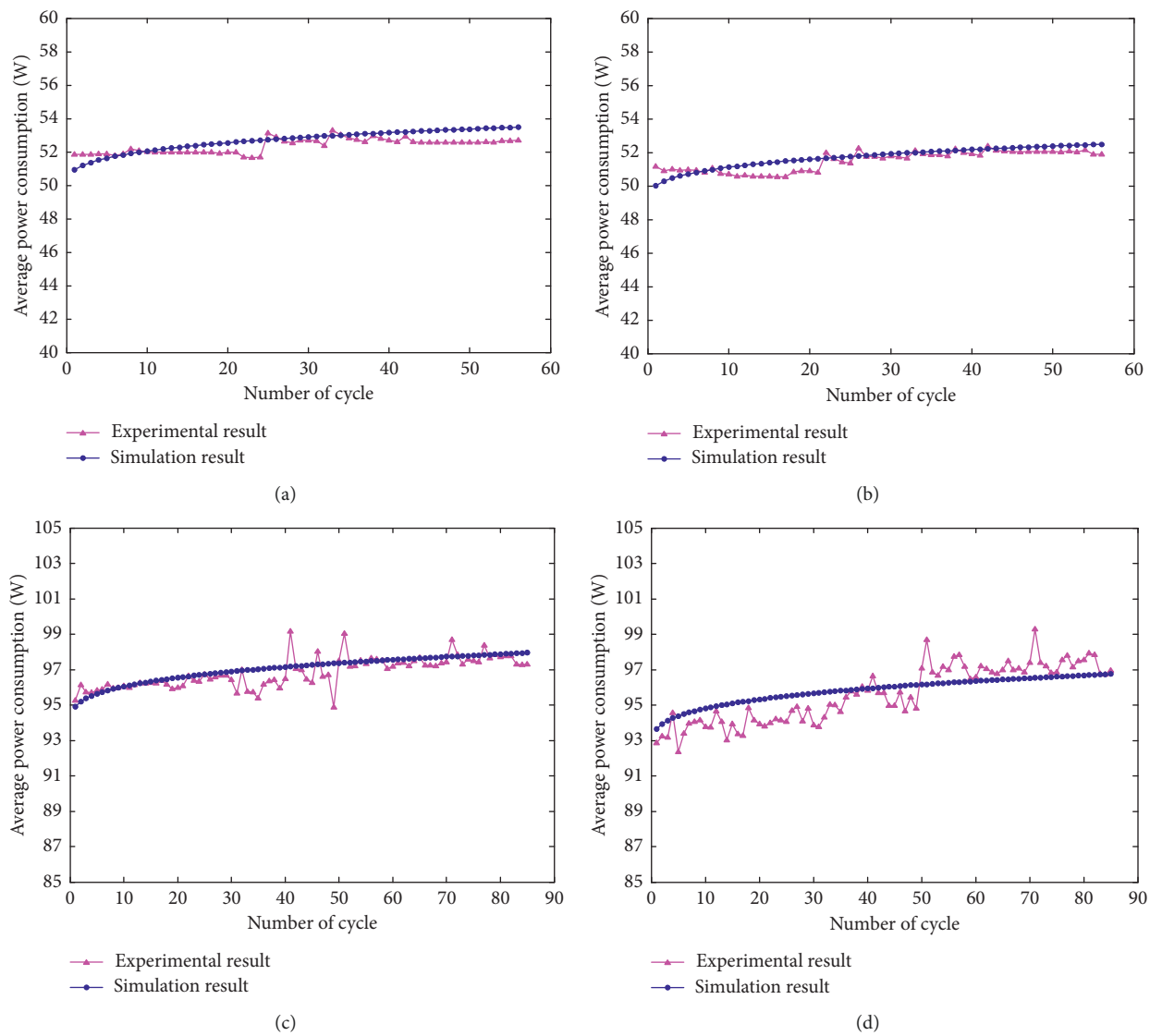

Figure 14: Simulation data of the average power consumption of the PTRs at upper heat reject temperature condition: (a, b) 1 W@60 K prototypes; (c, d) 5 W@80 K prototypes.

Table 5: Estimated values of the model parameters.

Parameters	Type A No. 1	Type A No. 2	Type B No. 1	Type B No. 2
P_0	48.25	47.34	92.29	91.06
α_1	0.2673	0.2656	0.2639	0.2716
α_2	0.0830	0.0798	0.0778	0.0756
β	76.7335	83.2887	71.2825	68.9857

Table 6: Predicted lifetimes of the PTRs under thermal cycling condition.

Prototype	Cycle to failure (N_f)	Lifetime prediction (hour)
Type A No. 1	690	115900
Type A No. 2	753	126500
Type B No. 1	733	123100
Type B No. 2	748	125600

for small samples and strong robustness of the test results. Therefore, this paper uses the K-S test method to test the hypothesis of Weibull distribution. The K-S test method depends on the distance, D, between the EDF $F_n(t_i)$ and the TDF (theoretical distribution function) $F_0(t_i)$. We compare D with the critical value $D_{n,\alpha}$. If $D < D_{n,\alpha}$, the original hypothesis is accepted; otherwise, the original hypothesis will be rejected.

$$D = \max\left\{\left|F_0(t_i) - F_n(t_i)\right|\right\} = \max\{d_i\}, \tag{19}$$

where $d_i = \max\{|F_0(t_i) - ((i-0.3)/(n+0.4))|\} = \max\{|0.3789, 0.2507, 0.0569, -0.1594|\} = 0.3789$.

Therefore, $D < D_{4,0.05} = 0.6239$, the original hypothesis is accepted, which means the failure time data of the PTRs follow the two-parameter Weibull distribution.

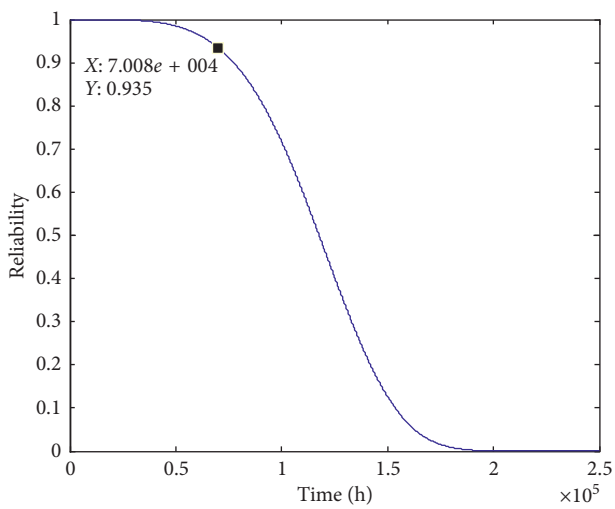

Figure 15: Reliability curve of SPTRs.

4.4.2. Reliability Calculation. The reliability estimation of the PTRs can be calculated by equation (17) $R_L = \exp[-(t^m/2t^*)\chi^2_\gamma(2r+2)]$, where the parameter γ is the confidence level and we assumed that $\gamma = 0.75$, $\chi^2_\gamma(\cdot)$ is the chi-Squared distribution and $\chi^2_\gamma(2r+2) = \chi^2_{0.75}(2\times 4+2) = \chi^2_{0.75}(10) = 6.737$. Then, the result of the reliability estimation of the PTRs at lower confidence limit is presented in Figure 15. The reliability of the PTRs at lower confidence limit of 0.75 is 0.935 at continuous operation for 8 years (70080 hours) under thermal cycling.

5. Conclusion

The 8 years designed lifetime of space PTRs have the challenge to maintain stable operation in despite of rigorous space environment. In this study, theoretical and experimental research on the thermal stability, lifetime prediction, and reliability estimation of PTRs in a thermal cycling environment is carried out. The ground vacuum thermal cycling tests for two types of space PTRs have been completed for about two years, and the effects of heat rejection temperature on thermal stability and dynamic performance of PTRs were investigated. Moreover, the innovative thermal cycling degradation model and reliability estimation methodology were established and validated to quickly and accurately assess the lifetime and reliability of the space PTRs. The reliability of the PTRs was obtained as 0.935 at continuous operation for 8 years under thermal cycling. The results show that performance and thermal stability of type A (1 W@60 K) and type B (5 W@80 K) PTRs meet the program requirements as expected, and the PTRs could fulfill the lifetime requirement of 8 years on orbit. Further investigation will continue to research the detailed performance degradation factors of the PTRs.

Data Availability

The data used to support the findings of this study are available from the corresponding author upon request.

Conflicts of Interest

The authors declare that they have no conflicts of interest.

Acknowledgments

This study was conducted as a part of a project supported by the National Natural Science Foundation of China (grant no. 51375487).

References

[1] R. G. Ross, "Requirements for long-life mechanical cryocoolers for space application," *Cryogenics*, vol. 30, no. 3, pp. 233–238, 1990.

[2] T. Conrad, B. Schaefer, L. Bellis, R. Yates, and M. Barr, "Raytheon long life cryocoolers for future space missions," *Cryogenics*, vol. 88, pp. 44–50, 2017.

[3] J. He, Y. Guo, J. Miao et al., "Pre-flight thermal performance test of a 35 K cryogenic integrated system," *International Journal of Refrigeration*, vol. 98, pp. 372–380, 2019.

[4] R. Radebaugh, "Development of the pulse tube refrigerator as an efficient and reliable cryocooler," *Proceedings of the Institute of Refrigeration*, vol. 96, pp. 11–31, 2000.

[5] W. E. Gifford and R. C. Longsworth, "Surface heat pumping," *Advances in Cryogenic Engineering*, vol. 11, pp. 171–179, 1966.

[6] E. Tward, C. K. Chan, C. Jaco, J. Godden, J. Chapsky, and P. Clancy, "Miniature space pulse tube cryocoolers," *Cryogenics*, vol. 39, no. 8, pp. 717–720, 1999.

[7] N. Wang, M. Zhao, Y. Ou et al., "A high efficiency coaxial pulse tube cryocooler operating at 60 K," *Cryogenics*, vol. 93, pp. 48–50, 2018.

[8] F. Wan, Y. Tan, Z. Jiang, X. Chen, Y. Wu, and P. Zhao, "Lifetime prediction and reliability estimation methodology for Stirling-type pulse tube refrigerators by gaseous contamination accelerated degradation testing," *Cryogenics*, vol. 88, pp. 116–124, 2017.

[9] C. Liubiao, W. Xianlin, L. Xuming, P. Changzhao, Z. Yuan, and W. Junjie, "Numerical and experimental study on the characteristics of 4 K gas-coupled stirling-type pulse tube cryocooler," *International Journal of Refrigeration*, vol. 88, pp. 204–210, 2018.

[10] H.-U. Oh, M.-K. Lee, S. Shin, and J.-S. Hong, "A numerical and experimental investigation of the thermal control performance of a spaceborne compressor assembly," *Cryogenics*, vol. 51, no. 9, pp. 477–484, 2011.

[11] R. G. Ross and D. L. Johnson, "Effect of heat rejection conditions on cryocooler operational stability," *Advances in Cryogenic Engineering*, vol. 43, pp. 1745–1752, 1998.

[12] T. Nguyen, J. Russo, G. Basel et al., "Northrop Grumman HEC flight coaxial cryocoolers performance," in *Tri-Technology Device Refrigeration*, Vol. 10626, Proceedings of SPIE, Bellingham, WA, USA, 2018.

[13] Y. Sato, K. Shinozaki, K. Sawada et al., "Outgas analysis of mechanical cryocoolers for long lifetime," *Cryogenics*, vol. 88, pp. 70–77, 2017.

[14] T. C. Nast, E. Roth, J. R. Olson et al., "Qualification of lockheed martin micro pulse tube cryocooler to TRL6," *Cryocoolers*, vol. 18, pp. 45–50, 2014.

[15] J. M. Cauquil, J. Y. Martin, P. Bruins, and A. A. J. Benschop, "Update on life time test results and analysis carried out on thales cryogenics integral coolers (RM family)," in *Proceedings of the SPIE-The International Society for Optical Engineering*, vol. 7, pp. 52–59, Seattle, WA, USA, 2003.

[16] K. Shirey, S. Banks, R. Boyle, and R. Unger, "Design and qualification of the AMS-02 flight cryocoolers," *Cryogenics*, vol. 46, no. 2-3, pp. 143–148, 2006.
[17] J. M. Cauquil, J. Y. Martin, P. Bruins et al., "MTTF prediction in design phase on thales cryogenics integral coolers," *Cryocoolers*, vol. 12, pp. 87–94, 2003.
[18] Y.-L. He, D.-W. Zhang, W.-W. Yang, and F. Gao, "Numerical analysis on performance and contaminated failures of the miniature split stirling cryocooler," *Cryogenics*, vol. 59, pp. 12–22, 2014.
[19] E. D. Marquardt, "Cryocooler reliability issues for space applications," *Cryogenics*, vol. 41, no. 11-12, pp. 845–849, 2001.
[20] G. Davey, "Review of the oxford cryocooler," *Advances in Cryogenic Engineering*, vol. 35, pp. 1423–1430, 1990.
[21] E. Marquardt and R. Radebaugh, "Design optimization of linear-arm flexure bearings," *Cryocoolers*, vol. 8, pp. 293–304, 1995.
[22] C. Chan, T. Nguyen, C. Jaco, B. J. Tomlinson, and T. Davis, "High capacity two-stage pulse tube cooler," *Cryocoolers*, vol. 12, pp. 219–224, 2003.
[23] S. W. K. Yuan and D. T. Kuo, "Cryocooler contamination study: temperature dependence of outgassing," *Cryocoolers*, vol. 11, pp. 659–664, 2001.
[24] S. W. K. Yuan, D. T. Kuo, and A. S. Loc, "Cryocooler contamination study," *Advances in Cryogenic Engineering*, vol. 45A, 2000.
[25] Y. Cheng and E. A. Elsayed, "Reliability modeling of mixtures of one-shot units under thermal cyclic stresses," *Reliability Engineering and System Safety*, vol. 167, pp. 58–66, 2017.
[26] C. Zehua and Z. Shurong, "Lifetime distribution based degradation analysis," *IEEE Transactions on Reliability*, vol. 54, no. 1, pp. 3–10, 2005.
[27] A.-M. Deng, X. Chen, C.-H. Zhang et al., "Reliability assessment based on performance degradation data," *Journal of Astronautics*, vol. 27, pp. 546–552, 2006.
[28] M. Hanes, "Performance and reliability improvements in a low-cost stirling cycle cryocooler," *Cryocoolers*, vol. 11, pp. 87–95, 2001.
[29] X. P. Chen, M. Xia, L. Y. Wang et al., "The reliability development of miniature stirling cryocoolers," *Cryocooler*, vol. 18, pp. 601–607, 2014.
[30] K. C. Datsiou and M. Overend, "Weibull parameter estimation and goodness-of-fit for glass strength data," *Structural Safety*, vol. 73, pp. 29–41, 2018.